Random-deposition models for thin-film epitaxial growth

J. W. Evans
Ames Laboratory and Department of Physics, Iowa State University, Ames, Iowa 50011
(Received 2 November 1988)

The simple on-top site random-deposition model for film growth on a simple-cubic (100) substrate is extended to other adsorption-site geometries and crystal structures. Nontrivial statistical correlations within the growing film typically result. However, the master equations can be solved exactly to elucidate, e.g., growth kinetics, Bragg intensity (I_{Br}) behavior for surface diffraction, and spatial correlations within the film. Other techniques facilitate analysis of the percolative structure of intralayer islands. For random deposition at fourfold hollow sites on a face-centered cubic (100) substrate, despite the absence of diffusion, there are distinct I_{Br} oscillations similar to those observed experimentally during deposition of Pt on Pd(100) at low temperature.

I. INTRODUCTION

Epitaxial growth of thin films has become an area of much current research, because of both its fundamental interest and also its importance in device fabrication. A variety of statistical mechanical models have been developed which describe such processes. These include the following.

(i) The random deposition model for growth on the (100) face of a simple-cubic crystal [sc(100)] or (10) face of a 2D (two dimensional) square lattice [sq(10)]:[1,2] Atoms are randomly deposited at constant rate on top of previously occupied sites. Clearly there are no overhangs, columns grow independently, and their height statistics is Poisson. Thus the surface width ξ of the film scales like $\langle h \rangle^{1/2}$, as $\langle h \rangle \to \infty$, where $\langle h \rangle$ is the mean height (i.e., the total coverage Θ).

(ii) Ballistic deposition models for sc(100) or sq(10) growth:[3,4] Here a "vertical rain" of atoms stick at the first empty site reached with a filled nearest neighbor (NN). Overhangs and avoids result. If L is the substrate linear dimension then $\xi \sim \langle h \rangle^{\beta}$ with $L = \infty$, and $\xi \sim L^{\alpha}$ with $\langle h \rangle = \infty$. The exponents α, β are nontrivial and dimension dependent. Allowing multiple restructuring after hitting may change these exponents.[4]

(iii) The Eden model assumes equal addition probabilities for all empty sites neighboring filled sites.[3,4] Overhangs and voids again result, and exponents α, β assume values for ballistic deposition (with no restructuring). This scaling reflects long-wavelength fluctuations.[5]

(iv) Kinetic solid-on-solid (SOS) models[2,6] assume no overhangs and simple interactions between atoms. Equilibrium SOS models exhibit a roughening transition at some temperature $T_R > 0$, above which the height $h(\mathbf{r})$ at lateral position $\mathbf{r}$ satisfies $\langle |h(\mathbf{r}) - h(\mathbf{0})|^2 \rangle \sim |\mathbf{r}|$ in 2D and $\ln|\mathbf{r}|$ in 3D. The kinetic model introduces dynamics through microscopic absorption, desorption, and diffusion mechanisms. It describes the transition from nucleated growth for $T \lesssim T_R$ to continuous growth for $T \gtrsim T_R$. For the latter, steady states with constant (or periodic) $d\langle h \rangle / dt$ and ξ occur.

(v) Cluster statistics models describing structure only, not dynamics, involve counting certain interface configurations of N atoms.[7] These relate to deposition models as random animals relate to kinetic cluster growth models.[8]

(iv) Terrace statistics models, mostly for 1D substrates, describe structure only, not dynamics. Finite-level models may describe the initial stages of epitaxy or near layer-by-layer growth.[9] Infinite-level models may describe perfect or disordered vicinal surfaces.[10] *Ad hoc* specifications of terrace width distributions, and/or probabilities for stepping up or down, allow straightforward calculation of diffracted intensity profiles. Simple generalizations for 2D substrates have been proposed.[11]

Often thin-film growth is monitored utilizing surface-sensitive diffraction techniques.[12] In a kinematic scattering theory, the diffracted intensity profile is determined by the pair-correlation function of the scatterers or "surface atoms." Here we consider only the amplitude of the Bragg peak I_{Br} which is determined by the *net* fraction of scatterers S_j in the various layers j as[12]

$$I_{Br} = \left| \sum_j S_j e^{ij\phi} \right|^2 . \tag{1}$$

Here ϕ is the phase angle between scattering from adjacent layers. I_{Br} is most sensitive to interface structure near the anti-Bragg condition $\phi = (2n+1)\pi$, where $e^{ij\phi} = (-1)^j$. The appearance of intensity (I_{Br}) oscillations during "near" layer-by-layer growth is now exploited routinely as an analytic tool. Specifically, reflection high-energy electron diffraction is often used during molecular beam epitaxy to monitor the total coverage in near layer-by-layer epitaxial growth.[12] If one makes the common assumption[9-12] that each atom produces a net shielding of one atom in the adlayer directly beneath, then $S_j \equiv \Theta_j - \Theta_{j+1}$ where Θ_j is the coverage of layer j. The same result follows from an alternative prescription described below.

Here we extend the random-deposition model to other absorption-site geometries and crystal structures. Specifically we consider random deposition at bridge sites

for a 1D substrate, and at the fourfold hollow sites starting from the (100) face of a face-centered-cubic (fcc) crystal. The fourfold hollow adsorption-site requirement is certainly natural for isomorphic fcc crystal growth, since it reflects crystal geometry. Analysis of this type of model is motivated by recent experiments on the deposition of Pt on Pd(100) at low temperatures.[13,14] Our work provides a new class of epitaxial-growth models which are *exactly solvable,* but not trivial as is the sc(100) random-deposition model. In the new models, the geometry of the adsorption-site requirement produces correlations within layers as the film grows. Resulting growth kinetics and structure is nontrivial and will be analyzed in the following sections together with the associated behavior of I_{Br}.

In Sec. II we briefly describe a rate-equation analysis of the sc(100) random-deposition model and discuss associated I_{Br} behavior. The rate-equation approach is adapted to provide an exact analysis of the kinetics and correlated statistics of random deposition at bridge sites on a 1D substrate in Sec. III and at the fourfold hollow sites on a fcc(100) substrate in Sec. IV. (These rate equations are just the hierarchical form of the master equations.) Specifically we focus on elucidating the behavior of the Θ_j, the short-range intralayer correlations, and the associated I_{Br}. In Sec. V we characterize the (nonlocal) structure of the islands or clusters of filled sites within each layer exploiting concepts and techniques of percolation theory. Surface structure is also discussed briefly. Some simple generalizations of these models which still permit exact analysis are described in Sec. VI. There we also indicate the difficulties inherent in rate-equation analysis of other thin-film growth models. Finally in Sec. VII we review our findings.

II. THE sc(100) RANDOM DEPOSITION MODEL

Let k denote the rate of random deposition on top of previously occupied sites, starting from a sc(100) substrate at time $t=0$. Here and in the following sections, we label the top substrate layer by $j=0$ (so $\Theta_0=1$) and higher layers by $j>0$. Since the total number of adsorption sites is constant in this model, the total coverage $\Theta=\sum_{j=1}^{\infty}\Theta_j$ equals kt. The rate of change of Θ_j is determined by the fraction of columns $S_{j-1}=\Theta_{j-1}-\Theta_j$ of height $j-1$ through

$$d/dt\,\Theta_j = kS_{j-1}\ . \tag{2}$$

The solution (2) satisfies[1,2] $\Theta_j=\sum_{k=j}^{\infty}S_k$ with $S_k=\Theta^k e^{-\Theta}/k!$. Note that if f_j is defined via $\Theta_{j+1}=f_j(\Theta_j)$, then from Stirling's formula, $x-f_j(x)=O(j^{-1/2})$ uniformly in x, as $j\to\infty$. From the above results for S_j, one can immediately calculate the Bragg intensity using (1). At the anti-Bragg condition, one finds that

$$I_{Br}=e^{-4\Theta} \tag{3}$$

exhibits *no* oscillations since this process is so far from layer-by-layer growth. Finally we remark that since this model describes the growth of independent columns, the above results hold for any substrate dimension.

III. RANDOM DEPOSITION AT BRIDGE SITES

Consider random deposition, with impingement rate k, at bridge sites, starting from a perfect 1D substrate at $t=0$. Figure 1 portrays the resulting film geometry. Note that for a site in layer j to be filled, a triangular "cone" of $K(j)=\sum_{i=1}^{j}i=j(j+1)/2$ atoms must be filled. Clearly, if the cones associated with two particular sites in the film intersect, then the occupancies of those sites will be *correlated.* We shall provide a more detailed discussion of these correlations below, but here we only wish to emphasize that they introduce a nontrivial structural complexity to the model which was absent from that of Sec. II.

Despite this fact, it is possible to recursively solve exactly the hierarchy of rate equations of the Θ_j and the various subconfiguration probabilities to which these couple. Clearly the statistics of the first layer is random, and $d\Theta_1/dt=k(1-\Theta_1)$. The requirement of two adjacent first-layer atoms for second-layer deposition is reflected in the equation $d\Theta_2/dt=k(\Theta_1^2-\Theta_2)$. Determination of $\Theta_3,\Theta_4,\Theta_5,\Theta_6,\ldots$ requires $2,4,10,26,\ldots$ equations, respectively, in addition to those determining the preceding Θ_j. These numbers increase dramatically with j reflecting the greatly increasing number of configurations that must be considered for higher layers. Some of these equations are shown schematically in Fig. 2. Results from numerical integration of these are presented below.

Figure 3 shows the time dependence of the Θ_j, for $j\le 6$, and of the total deposition rate $d\Theta/dt$. The latter decreases initially like $k(1-\Theta)\sim ke^{-kt}$ to an apparent asymptotic limit of $\sim 0.5k$. A different representation of Θ_j behavior is provided through f_j defined by $\Theta_{j+1}\equiv f_j(\Theta_j)$. From Fig. 4, we see that $f_j\le f_{j+1}$ indicating that growth of successive layers is increasingly less layer-by-layer-like. This is a consequence of the increased clustering, described quantitatively below, in successively higher layers. Figure 5 shows the corresponding Θ dependence of I_{Br} calculated from the Θ_j assuming that each atom in layer j shields (a net of) one atom in layer $j-1$. Equivalent results are obtained if one assumes that an atom supporting (and thus obscured by) 0, 1, 2 atoms it the layer above has a scattering factor of 1, $\frac{1}{2}$, 0, respectively (see the Appendix). One finds very weak oscillations in I_{Br} here reflecting the fact that the bridge site-adsorption requirement makes growth somewhat more layer-by-layer-like than for the model of Sec.

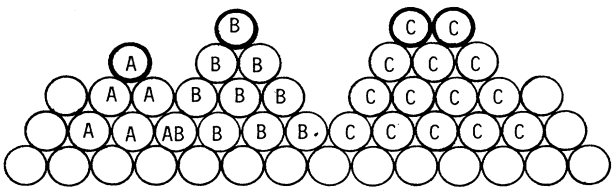

FIG. 1. Film geometry for random deposition at bridge sites. The cones associated with the third-layer atom A, fourth-layer atom B, and fourth-layer pair C, are indicated. Occupancies of the top A and B sites are correlated.

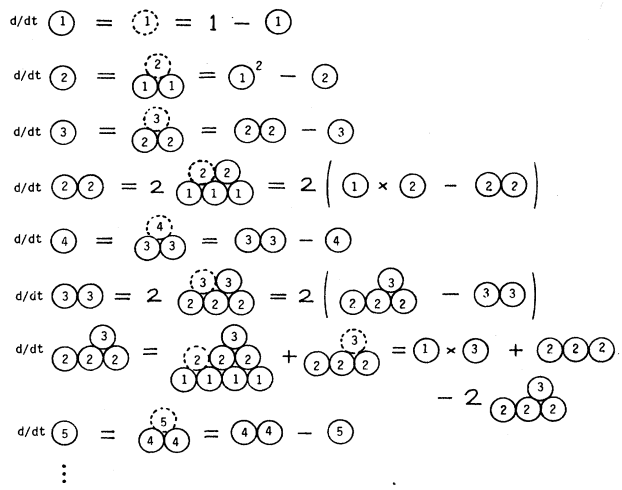

FIG. 2. Rate equations for random deposition at bridge sites with $k=1$. Probabilities of configurations are represented by the configurations themselves. Solid (dashed) circles represent filled (empty) sites in the layers indicated.

II. Here minima in I_{Br} occur at zeros of $1-2\Theta_1+2\Theta_2-\cdots$ (and I_{Br}), and maxima where $\Theta_1'-\Theta_2'+\Theta_3'-\cdots=0$.

Further insight into Θ_j and f_j behavior can be gleaned from the following.

(i) Short-time analysis. Let $K(\sigma)$ denote the number of atoms in the cone associated with the filled configuration σ, i.e., the number of atoms in σ plus the minimum number of additional deposited atoms required to support those in σ. Let $N(\sigma)$ denote the number of ways (physical orders of filling) of creating this cone. From analysis of the structure of the rate equations,[15] one can show that the probability of σ satisfies $P(\sigma)$

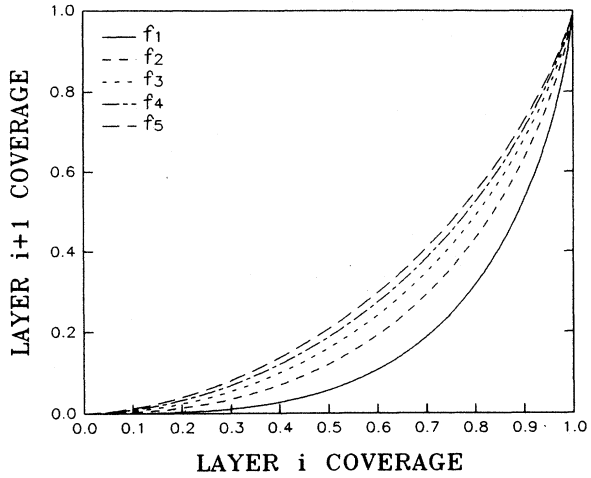

FIG. 4. $f_j(\Theta_j)\equiv\Theta_{j+1}$ for random deposition at bridge sites.

$\sim[N(\sigma)/K(\sigma)!](kt)^{K(\sigma)}$, as $t\to 0$. Thus one finds that

$$\Theta_j\sim\frac{N(j)}{K(j)!}(kt)^{K(j)}\quad\text{as } t\to 0\ , \tag{4}$$

where $K(j)=j(j+1)/2$, as previously, and $N(1)=1$, $N(2)=2$, $N(3)=16$, etc. Of course, the utility of (4) is greatly reduced with increasing j.

Equation (4) implies that $f_j(x)$ scales like $x^{(j+2)/j}$, and thus like $\hat{f}_j(x)\equiv f_1(x)^{(j+2)/3j}$, for small x. In fact, Table I shows that $f_j(x)/\hat{f}_j(x)$ is roughly independent of $j\lesssim 5$ for all x and that

$$f_j(x)\approx a(x)f_1(x)^{(j+2)/3j}\ , \tag{5}$$

where $a(x)$ varies monotonically from $a(0)\approx 0.4$ to $a(1)=1$. However, since the surface width diverges as

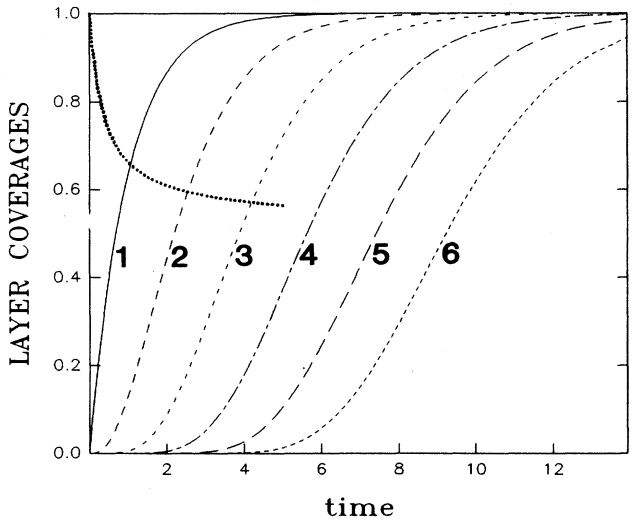

FIG. 3. Time dependence (in units of kt) of Θ_j (in monolayers) and $d\Theta/d(kt)$ (dotted line) for random deposition at bridge sites.

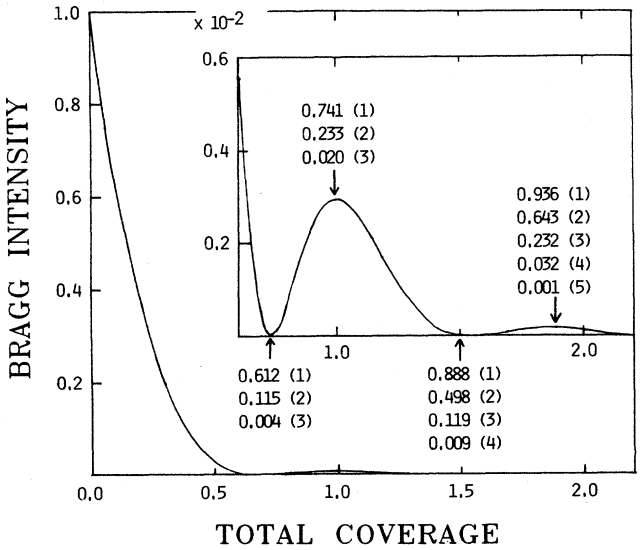

FIG. 5. Coverage dependence of I_{Br} for random deposition at bridge sites. Layer coverages at maxima and minima are shown; (j) indicates layer j.

TABLE I. Values of $f_j(x)/\hat{f}_j(x)$ for the bridge-site deposition model.

x	$\frac{1}{8}$	$\frac{1}{4}$	$\frac{3}{8}$	$\frac{1}{2}$	$\frac{5}{8}$	$\frac{3}{4}$	$\frac{7}{8}$
$j=2$	0.624	0.699	0.760	0.813	0.863	0.911	0.958
$j=3$	0.551	0.646	0.721	0.790	0.846	0.903	0.957
$j=4$	0.532	0.635	0.715	0.785	0.848	0.907	0.962
$j=5$	0.528	0.636	0.721	0.791	0.855	0.914	0.966

$j\to\infty$, one expects that $\Theta_{j+1}\sim\Theta_j$, and so $f_j(x)\sim x$, as $j\to\infty$. This behavior is not incorporated in (5).

(ii) Long-time analysis. Exact integration of the rate equations reveals that probabilities $P(\sigma)$ of filled configurations σ are given by linear combinations of terms $t^p e^{-qt}$ with integer p and q. One can readily identify the form of the dominant term in $1-P(\sigma)$ as $t\to\infty$. In particular, one finds that

$$\Theta_j \sim 1-\frac{(2t)^{j-1}}{(j-1)!}e^{-t} \quad \text{as } t\to\infty \ , \tag{6}$$

and if σ has n-filled sites in its *uppermost* layer j then $P(\sigma)\sim\Theta_j^n$ as $t\to\infty$. From (6), it follows immediately that

$$f_j(x)\sim 1+(2/j)(1-x)\ln(1-x) \quad \text{as } x\to 1 \ .$$

In fact one can show that

$$f_1(x)\equiv 2T_2[(1-x)\ln(1-x)] \ ,$$

where $T_m[g]$ removes terms x^n, with $n\le m$, from the Taylor expansion of $g(x)$.

Finally we provide a detailed analysis of spatial correlations within the growing film. Clearly if the cones associated with two sites within the film intersect, then the pair probability for both to be filled will exceed the product of the corresponding pair of layer coverages. (Less "supporting" atoms are required for these sites to be filled than if they were far separated.) These positive correlations correspond to *clustering* induced by the geometric aspects of the kinetic model rather than by attractive interactions, which are absent here. Specifically, consider the intralayer pair correlations, $C_j(l)\equiv P_l(j\text{-}j)-P(j)^2$, where $P_l(j\text{-}j)$ is the probability of a pair of layer-j atoms separated by l lattice vectors and $P(j)\equiv\Theta_j$. These are nonzero only for the finite range $l\le j-1$ (see Fig. 6), which demonstrates the non-Markovian nature of the film statistics for $j\ge 2$ (see below). Figure 7 shows the Θ_j dependence of the NN correlations $C_j(1)$. Divergence of the surface width as $j\to\infty$, together with the geometric bound on the surface slope of $\pi/4$, suggest the creation of increasingly longer stretches of layer-j atoms for fixed Θ_j as $j\to\infty$. This implies divergence of the intralayer correlation length, so $C_j(l)\to\Theta_j(1-\Theta_j)$ for all l as $j\to\infty$.

In general, two-cluster correlations will be positive if the cones associated with the constituent clusters of sites intersect (Fig. 1) and will be zero otherwise. The latter result, which follows from the rate equations, allows factorization of corresponding configuration probabilities and has been exploited to reduce the number of equations required for determination of the Θ_j's. Note, however, that the statistics of nonfactorizing clusters of sites is quite nontrivial. Let $P(j)\equiv\Theta_j, P(jj), P(jjj), \ldots$ denote the probability of finding one, two, three, ... consecutive filled sites in layer j. One finds that $P(jjj)-P(jj)^2/P(j)$ are nonzero but small for $j\ge 2$, with maxima of 2.2×10^{-4}, 1.2×10^{-3}, 2.2×10^{-3} at $\Theta_j=0.55$, 0.63, 0.63, for $j=2$, 3, 4, respectively. Thus the statistics of higher ($j\ge 2$) layers do not satisfy an exact Markov property, as often assumed in terrace statistics models.[9–11] We also calculate the Ursell-Mayer three-point correlations[16]

$$C(jjj)\equiv P(jjjj)-2P(jj)P(j)-P(j-j)P(j)+2P(j)^3 \ .$$

These achieve maxima of 4.6×10^{-3}, 6.5×10^{-3}, 9.2×10^{-3} at $\Theta_j=0.44$, 0.31, 0.28 for $j=2$, 3, 4, respectively.

IV. RANDOM DEPOSITION AT FOURFOLD HOLLOW SITES

Consider random deposition, at impingement rate k, at fourfold hollow sites starting from an fcc(100) substrate at $t=0$. Figure 8 portrays resulting film geometry. For a site in layer j to be filled, a pyramidal cone of $K(j)=\sum_{i=1}^{j} i^2=j(j+1)(2j+1)/6$ atoms is required. If cones associated with two sites intersect, then their occupancies will be *correlated.* Thus nontrivial structural

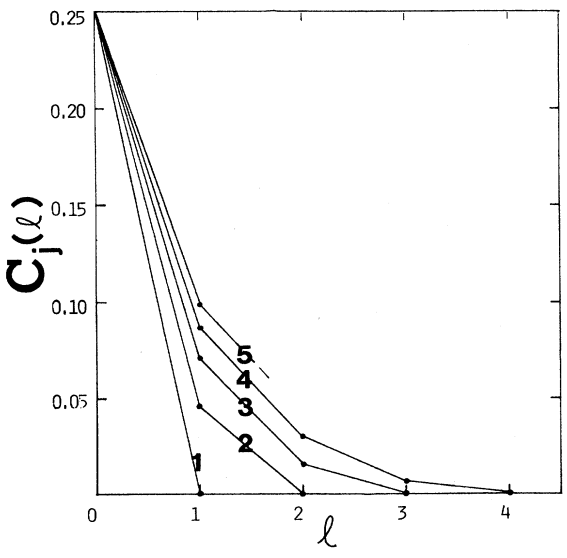

FIG. 6. Intralayer pair correlations for half-filled layers ($\Theta_j=\frac{1}{2}$) for $1\le j\le 5$.

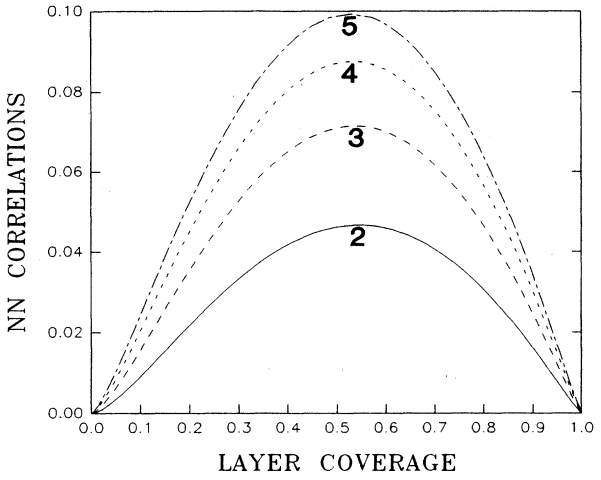

FIG. 7. Dependence of $C_j(1)$ on Θ_j, for $2 \leq j \leq 5$.

complexity results in this model as for that of Sec. III. Again one can recursively solve the rate equation for the Θ_j and various subconfiguration probabilities to which these couple. The statistics of the first layer is random, and $d\Theta_1/dt = k(1-\Theta_1)$. The fourfold hollow adsorption-site requirement is reflected in the equation $d\Theta_2/dt = k(\Theta_1^4 - \Theta_2)$. Determination of $\Theta_3, \Theta_4, \ldots$ requires 5, 89, . . . equations, respectively, in addition to those determining the preceding Θ_j (see Fig. 9). These numbers increase more quickly than in Sec. III reflecting the greater number of configurations in the higher dimensions. Results from numerical integration of these equations are presented below.

Figure 10 shows the time dependence of Θ_j for $j \leq 4$ and of $d\Theta/dt$. The latter decreases initially like $k(1-\Theta) \sim ke^{-kt}$ to an apparent asymptotic limit of $\sim 0.4k$. Set $\Theta_{j+1} \equiv f_j(\Theta_j)$, as previously. Then Fig. 11 shows that $f_j \leq f_{j+1}$ indicating less layer-by-layer growth in successive layers, just as in Sec. III. Figure 12 shows the Θ dependence of I_{Br}, calculated from the assumption that each atom in layer i shields a net of one in layer $i-1$, or equivalently, that each atom supporting k atoms in the layer above has a scattering factor of $(4-k)/4$ for

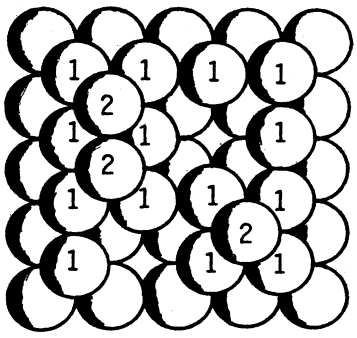

FIG. 8. Film geometry for random deposition at fourfold hollow sites. Layer-1 and -2 atoms are indicated.

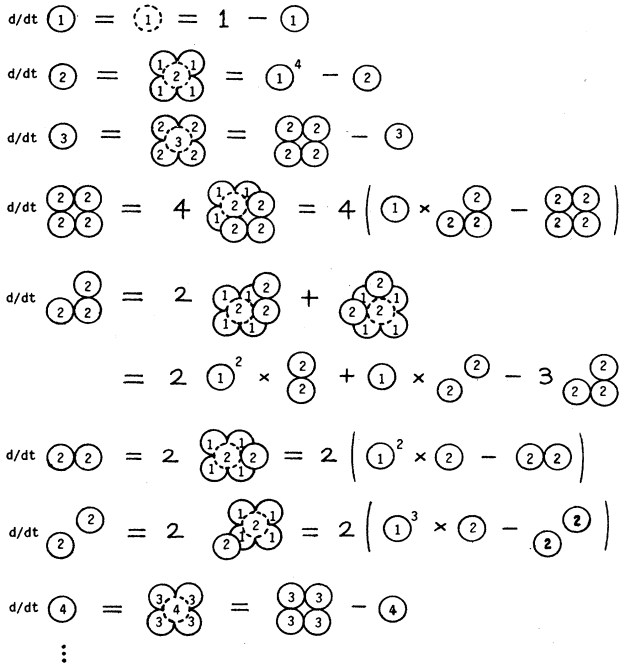

FIG. 9. Rate equations for random deposition at fourfold hollow sites with $k = 1$ (notation as in Fig. 2).

$0 \leq k \leq 4$ (see the Appendix). Oscillations in I_{Br} are now quite noticeable since the fourfold hollow adsorption-site requirement means that film growth is initially much more layer-by-layer-like than in the models of Secs. II and III. Minima occur where $1-2\Theta_1+2\Theta_2-\cdots$ (and I_{Br}) $=0$, and maxima where $\Theta_1'-\Theta_2'+\Theta_3'-\cdots=0$. This I_{Br} behavior matches quite closely the low-energy electron-diffraction Bragg intensity variations observed

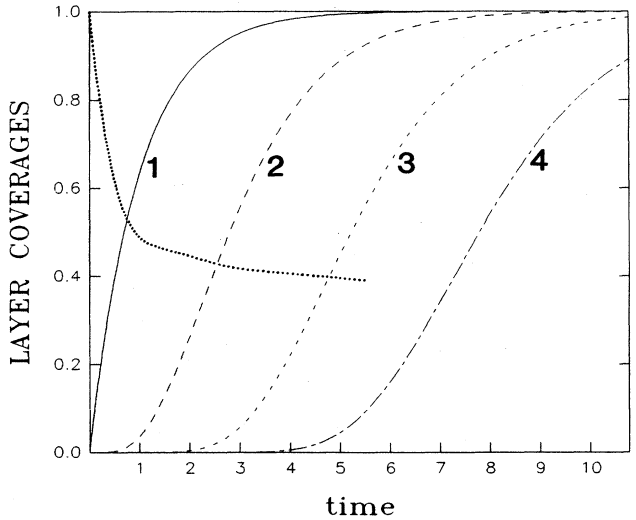

FIG. 10. Time dependence (in units of kt) of Θ_j (in monolayers) and $d\Theta/d(kt)$ (dotted line) for random deposition at fourfold hollow sites.

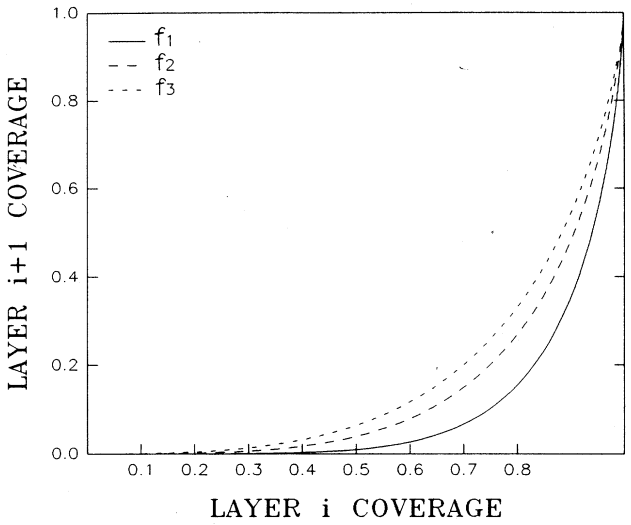

FIG. 11. $f_j(\Theta_j)\equiv\Theta_{j+1}$ for random deposition at fourfold hollow sites.

experimentally during growth of an epitaxial thin film of Pt on Pd(100) at low temperature.[13,14] As a consequence we can, e.g., accurately calibrate the coverage from I_{Br} measurements: $\Theta=0.89$ ($\Theta_1=0.77$, $\Theta_2=0.02$) at the first maximum, and $\Theta=1.82$ ($\Theta_1=0.97$, $\Theta=0.70$, $\Theta_3=0.15$) at the second.

Short- and long-time analysis of the rate equations again provide further insight into Θ_j and f_j behavior. In fact, Eq. (4) is still valid but now with $K(j)=j(j+1)(2j+1)/6$, and $N(j)$ giving the number of physical ordered fillings of a pyramid of $K(j)$ sites, so $N(1)=1$, $N(2)=24$, $N(3)=25\,159\,680$, etc. Thus $f_j(x)$ scales like $x^{K(j+1)/K(j)}$, and thus like

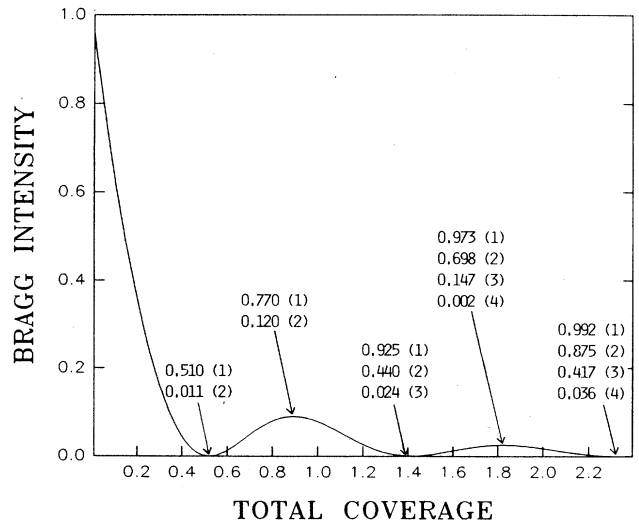

FIG. 12. Coverage dependence of I_{Br} for random deposition at fourfold hollow sites. Layer coverages at maxima and minima are shown (cf. Fig. 5).

$$\hat{f}_j(x)\equiv f_1(x)^{(2j^2+7j+6)/(10j^2+5j)},$$

for small x. Table II shows $f_j(x)/\hat{f}_j(x)$ values indicating that $f_j(x)\approx a(x)\hat{f}_j(x)$ at least for small j, where $a(x)$ varies from $a(0)\approx 0.15$ to $a(1)=1$. However divergence of the surface width again implies that $f_j(x)\sim x$ as $j\to\infty$. One can also show that

$$\Theta_j\sim 1-\frac{(4t)^{j-1}}{(j-1)!}e^{-t} \quad \text{as } t\to\infty, \tag{7}$$

and that $P(\sigma)\sim\Theta_j^n$ for a filled configuration σ with n sites in its uppermost layer j. In this model one finds that

$$f_j(x)\sim 1+(4/j)(1-x)\ln(1-x) \quad \text{as } x\to 1$$

and that $f_1(x)=4T_4[(1-x)\ln(1-x)]$, with T_m as in Sec. III.

Here, just as in Sec. III, the two-cluster correlations are positive if cones associated with the constituent clusters intersect and are zero otherwise. Specifically, the intralayer pair correlations $C_j(\boldsymbol{l})$ for a pair of layer-j atoms separated by $\boldsymbol{l}=(l_x,l_y)$ lattice vectors are nonzero only for $\max(|l_x|,|l_y|)\le j-1$. Figure 13 shows the Θ_j dependence of all nonzero $C_j(\boldsymbol{l})$ for $j\le 3$. These $C_j(\boldsymbol{l})$ values are determined by intergrating equations for 182 different configuration probabilities. The arguments of Sec. III again apply, suggesting divergence of the intralayer correlation length as $j\to\infty$. The above condition for vanishing of two-cluster correlations has the following implications for configurations in the second layer: If two clusters of filled sites are not linked by first or second NN bonds, then the configuration probability factorizes. Again this feature is used to reduce the number of equations required to determine the Θ_j's. The statistics of nonfactorizing clusters is generally complicated. There are only a few nontrivial identities, e.g., the following pairs of second-layer configurations have equal probabilities

$$\begin{matrix}2\cdot\cdot\\ \cdot 2\cdot\\ \cdot\cdot 2\end{matrix} \text{ and } \begin{matrix}2\cdot 2\\ \cdot 2\cdot\end{matrix},$$

$$\begin{matrix}\cdot 2\\ 2\cdot\\ 2\,2\end{matrix} \text{ and } \begin{matrix}2\cdot\cdot\\ \cdot 2\cdot\\ \cdot\,2\,2\end{matrix},$$

$$\begin{matrix}2\cdot 2\\ 2\,2\,2\end{matrix} \text{ and } \begin{matrix}2\cdot\cdot\\ 2\,2\,2\\ \cdot\cdot 2\end{matrix}.$$

Here the sites indicated by 2's are filled with second-layer atoms, and all others are unspecified. Table III shows errors associated with Kirkwood factorization for a variety of configurations and maximum amplitudes of associated Ursell-Mayer correlations.

TABLE II. Values of $f_j(x)/\hat{f}_j(x)$ for the fourfold hollow-site deposition model.

x	$\frac{1}{8}$	$\frac{1}{4}$	$\frac{3}{8}$	$\frac{1}{2}$	$\frac{5}{8}$	$\frac{3}{4}$	$\frac{7}{8}$
$j=2$	0.27	0.36	0.44	0.53	0.62	0.72	0.84
$j=3$	0.19	0.29	0.38	0.47	0.57	0.69	0.82

V. PERCOLATIVE INTRALAYER ISLAND STRUCTURE AND SURFACE STRUCTURE

The structure of filled clusters or islands of sites within each layer j is often of interest in nearly or exactly layer-by-layer epitaxial growth. Clearly as Θ_j increases, a critical average Θ_j^c, is reached at which these filled regions first link up sufficiently to span the substrate (the percolation threshold). At that point we shall argue (below) that the filled clusters have a ramified, fractal structure.

Henceforth, to be specific, we shall consider only the fcc(100) random-deposition model of Sec. IV, and somewhat arbitrarily define clusters as maximal sets of filled sites (within a given layer j) connected by NN bonds. Since the first layer ($j=1$) has random statistics, standard results from random-percolation theory apply to give $\Theta_1^c=0.593$ and to provide a characterization of the divergence of average cluster size, radius of gyration, etc., at Θ_1^c, and of the ramified, fractal cluster structure,[17,18] We expect that the intralayer correlations present in higher layers will not change the critical exponents characterizing the divergence of the average cluster size, etc., since the correlation length is always finite.[17,19] As a consequence, the fractal dimension of the percolation cluster at Θ_j^c should equal the random percolation value of $\frac{91}{48}$. However we do expect clustering to lower the percolation threshold and the cluster ramification (cluster perimeter length to size ratios).[19]

Small-cell real-space renormalization-group (RSRG) techniques[20] provide simple estimates of the Θ_j^c. The corresponding $\delta\Theta_j^c \equiv \Theta_j^c - \Theta_j^1$ values may provide semiquantitative estimates of deviations in the exact Θ_j^c from the exact random-percolation value of 0.593. (Hopefully systematic errors cancel.) From the exact horizontal spanning probabilities for 2×2 cells,[20] we obtain RSRG estimates of $\delta\Theta_2^c=-0.051$, $\delta\Theta_3^c=-0.074$, compatible with our expectations of lower threshold values. More reliable, and essentially exact determination of the Θ_j^c can be extracted from finite-size scaling (FSS) analysis in conjunction with computer simulation.[19,21] We obtain the FSS values $\delta\Theta_c^2=-0.049\pm0.001$, $\delta\Theta_3^c=-0.070\pm0.003$, $\delta\Theta_4^c=-0.089\pm0.005$, in surprisingly (perhaps accidentally) good agreement with RSRG results. FSS analysis also allows us to check the critical exponents. We always find random-percolation values confirming that a percolating cluster in layer j will have the random-percolation fractal dimension of $\frac{91}{48}$ at Θ_j. Figure 14 shows typical film geometries near the percolation thresholds of the first and fourth layers. Note that fourth-layer threshold clusters are "coarser" than the first-layer random percolation clusters, reflecting the development of positive correlations in the fourth layer. As an aside, we note that percolation thresholds for empty regions in layers $j>1$ must be determined independently, since the statistics of these is distinct from the filled regions.[22]

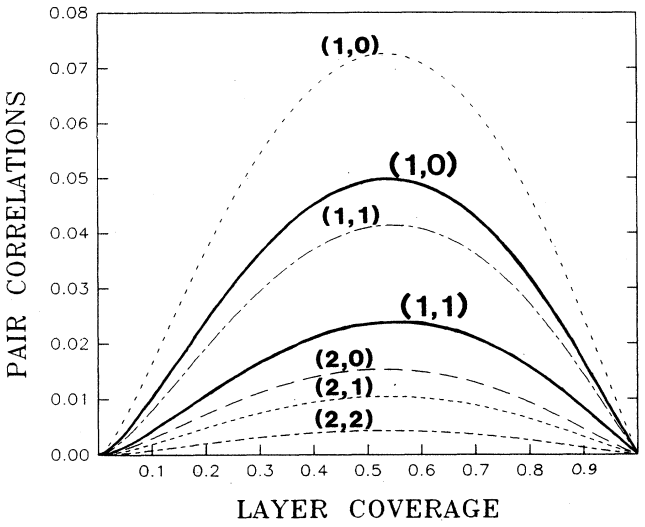

FIG. 13. Dependence of all nonzero $C_j(l)$ on Θ_j for $j=2$ (solid lines) and $j=3$.

Characterization of the surface structure of the growing film is also of interest. Figure 15 depicts the evolving surface profile during random deposition at fourfold hollow sites. One can clearly see the influence of the geometry of the adsorption site on the local or short-range structure. However, growth of regions of the film separated laterally by greater than $O(\langle h \rangle)$ lattice vec-

TABLE III. K: maximum errors for Kirkwood factorization of probabilities of various configurations in terms of probabilities of all constituent pair probabilities (except for *, indicating that only NN pairs were used). UM: maximum amplitudes of three-point (and four-point for $\frac{jj}{jj}$) Ursell-Mayer correlations. Θ_j values corresponding to maxima are given in parentheses. $[-m]$ means $\times10^{-m}$.

	jjj	$\frac{j}{jj}$	$\frac{j}{j\ j}$	$\frac{j}{jj}$	$\frac{j}{jj}$	$\frac{jj}{jj}$	$\frac{jj}{jj}$
K	2.5[−4]	1.1[−4]	5.1[−5]	−1.6[−2]	2.6[−3]*	−3.8[−2]	−8.5[−3]*
$j=2$	(0.53)	(0.55)	(0.57)	(0.60)	(0.70)	(0.65)	(0.64)
K	1.1[−3]			−3.1[−2]	4.9[−3]*	−8.2[−2]	−1.8[−2]*
$j=3$	(0.62)			(0.56)	(0.67)	(0.59)	(0.60)
UM	5.3[−3]	2.5[−3]	1.2[−3]	−9.5[−3]		6.0[−3]	
$j=2$	(0.44)	(0.44)	(0.44)	(0.73)		(0.79)	
UM	1.2[−2]			−1.6[−2]		8.6[−3]	
$j=3$	(0.43)			(0.75)		(0.83)	

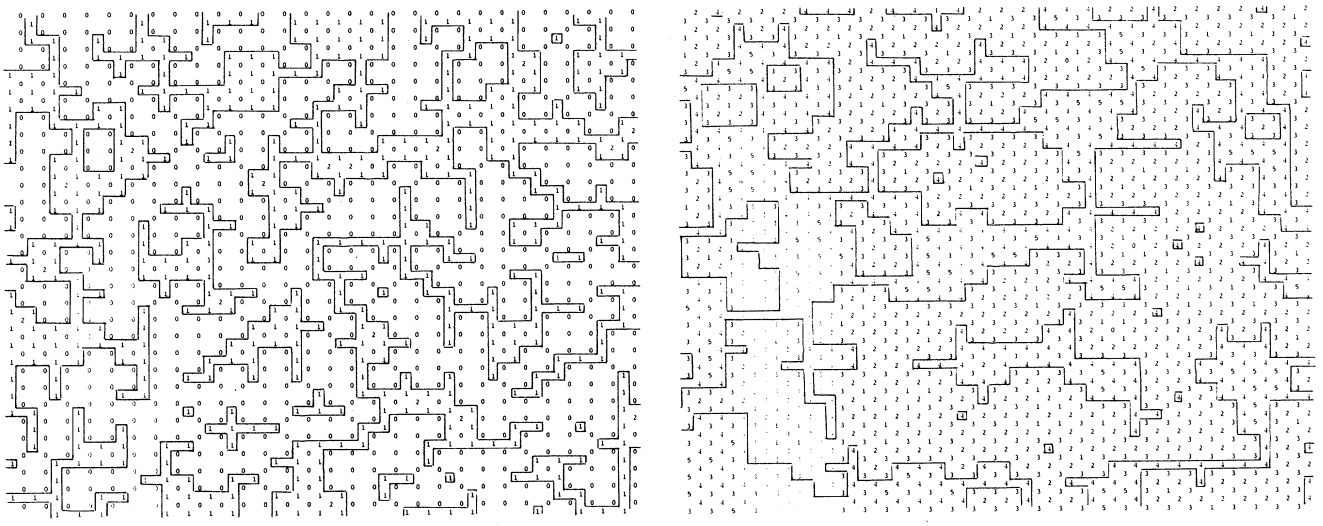

FIG. 14. Simulated film geometry near the percolation threshold for the first (fourth) layer is shown on the left (right). Layer-j atoms are indicated by j, and the lines indicate perimeters of layer-one (four) clusters.

tors is independent, so the Poisson result for surface width $\xi \sim \langle h \rangle^{1/2}$ may be expected to apply. This is also suggested by the analysis of Kardar *et al.*[5] We shall consider these questions in future work.

VI. OTHER SOLVABLE DEPOSITION MODELS

There is clearly considerable flexibility in the choice of adsorption-site requirement in random-deposition models. For example, we could modify the models of Secs. III and IV by demanding a larger "raft" of layer-i atoms surround the layer-$(i+1)$ adsorption site.

Consider, in general, random-deposition processes where the first-layer statistics is random, and layer-$(i+1)$ adsorption requires an ensemble of N-layer i atoms. For impingement rate k, one has that

$$d\Theta_1/dt = k(1-\Theta_1), \quad d\Theta_2/dt = k(\Theta_1^N - \Theta_2) , \tag{8}$$

independent of the configuration of the N-atom adsorption ensemble. The $d\Theta_i/dt$ for $i \geq 3$ do depend on this configuration. Clearly as N increases, the process becomes initially more layer-by-layer-like. Consider the point where $d\Theta_1/dt = d\Theta_2/dt$ which corresponds closely to the first maximum of $I_{\mathrm{Br}} \approx (1-2\Theta_1+2\Theta_2)^2$ for $N \geq 4$. Here one finds that Θ_1 (and Θ_2) equals 0.770 (and 0.120) for $N=4$, 0.789 (and 0.010) for $N=5$, 0.809 (and 0.089) for $N=6$, 0.838 (and 0.075) for $N=8$, 0.858 (and 0.065) for $N=10$, 0.868 (and 0.052) for $N=12$. Obviously the height of the first maximum increases with N.

Models involving random deposition at threefold hollow sites ($N=3$) of an fcc(111) substrate have been used to describe poor wetting and disorder at certain crystal-melt interfaces.[23] However, in these models, there is natural steric constraint that occupation of one substrate deposition site blocks occupation of the three NN sites.[23] Thus at most half these sites can fill, and for random deposition only 37.9% (Ref. 24) are filled at saturation. Clearly the statistics of the first layer is not random (and not exactly solvable), in contrast to all of the models developed above in this work. In fact, here the intralayer correlations have infinite range but fast superexponential decay.[25] Also, for these models, deposition in higher layers is typically not epitaxial.

Another simple model modification involves specifying different adsorption rates for the different layers. This results in no structural change in the hierarchical rate equations, so exact solution is again possible. In the growth of bimetallic thin films, it is conceivable that the rate of deposition onto the substrate differs slightly from

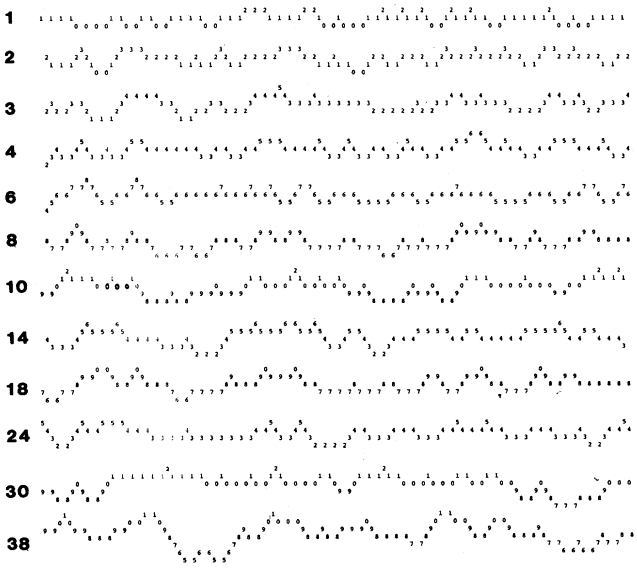

FIG. 15. Simulated thin-film surface profiles in the (1,1) direction for random deposition at fourfold hollow sites. The total coverage is indicated on the left, and layer-j surface atoms are denoted by j (modulo 10).

that for higher layers. Clearly increasing the former makes the process initially more layer-by-layer-like.

A key feature of the exactly solvable deposition models described above is that the state of a given layer is independent of the state of all higher layers. As a consequence, the hierarchical rate equations couple "downwards" only, making an exact solution viable. Ballistic deposition, Eden, and kinetic SOS models do not satisfy this property, i.e., $d\Theta_i/dt$ depends on the state of layer $i+1$ and sometimes higher layers. One could, however, remove this dependence in the sc(100) Eden model by imposing the additional constraint that attachment only occurs at empty sites with a filled NN beneath or in the same layer. One still has the complication that the hierarchical equations couple laterally to increasingly larger configurations (in contrast to our models). However one can still obtain exact results for $\Theta_1=1-e^{-kt}$ (trivially) and for Θ_2.[26]

VII. CONCLUSIONS

In this paper, we have extended the trivial sc(100) random-deposition model to other adsorption-site geometries and crystal structures. Although the resulting models incorporate nontrivial statistical correlations, one can still obtain exact results for layer coverages (and other quantities). It is clear that restrictions on the adsorption-site geometry, which are almost certainly operable in real physical systems, have a dramatic effect on the extent to which the initial film growth is layer-by-layer-like. Appropriate treatment of adsorption site geometry seems essential to an understanding of the Bragg intensity oscillations observed recently in experimental growth of Pt films on Pd(100) at cryogenic temperatures.[13,14] This observation motivated our analysis of the coverage dependence of the Bragg intensity in previous sections. Clearly a full-diffracted intensity-profile analysis is also of interest. In future work on the fourfold hollow-site random-deposition model, we shall show that the diffuse intensity has nontrivial angular dependence even before the second layer has significant population.[27] This contrasts the standard sc(100) model,[28] again showing the important influence of geometry.

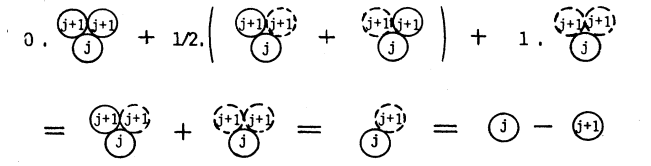

FIG. 16. Diagrammatic proof of (A1) for the bridge-site model $N=2$.

ACKNOWLEDGMENTS

Ames Laboratory is operated for the U.S. Department of Energy by Iowa State University under Contract No. W-7405-ENG-82. This work was supported by the Division of Engineering, Mathematics, and Geosciences with Budget Code No. KC-04-01-03. The author would also like to acknowledge P. A. Thiel for useful discussions and comments on the manuscript.

APPENDIX: SURFACE ATOM SCATTERING FACTORS

For the bridge-site deposition model, each atom can support (and thus be obscured by) up to $N=2$ atoms in the layer above. In the fourfold hollow deposition model, $N=4$. In either case, suppose that an atom supporting exactly k atoms in the layer above has a scattering factor $f_k=(N-k)/N$. Thus the scattering factor is zero (unity) for completely obscured (unobscured) atoms. Let $\Theta_j(k)$ denote the fraction of layer j atoms obscured by exactly k atoms in layer $j+1$. Then the net fraction of scatterers in layer j equals

$$S_j \equiv \sum_{k=0}^{N} f_k \Theta_j(k) = \Theta_j - \Theta_{j+1} . \tag{A1}$$

The last identity exploits probability relationships. These are illustrated in Fig. 16 for $N=2$, but the generalization is obvious. Note that for $j=0$ and random first-layer statistics, (A1) follows from the identity

$$\sum_{k=0}^{N} k \begin{bmatrix} N \\ k \end{bmatrix} (1-p)^k p^{N-k} = N(1-p) .$$

[1] F. Reif, *Statistical and Thermal Physics* (McGraw-Hill, New York, 1965), p. 42.

[2] J. D. Weeks, G. H. Gilmer, and K. A. Jackson, J. Chem. Phys. **65**, 712 (1976).

[3] P. Meakin, CRC Crit Rev. Solid State Mat. Sci. **13**, 143 (1988).

[4] P. Meakin and R. Jullien, in *Modeling of Optical Thin Films*, edited by M. R. Jacobson [Proc. SPIE **821**, 46 (1988)].

[5] M. Plischke and Z. Ratz, Phys. Rev. A **32**, 3825 (1985); J. Kertesz and D. E. Wolf, J. Phys. A **21**, 747 (1988); M. Kardar, G. Parisi, and Y.-C. Zhang, Phys. Rev. Lett. **56**, 889 (1986).

[6] J. D. Weeks and G. H. Gilmer, Adv. Chem. Phys. **40**, 157 (1979).

[7] H. M. V. Temperley, Proc. Cambridge Philos. Soc. **48**, 683 (1952); V. Privman and N. M. Svrakic, J. Stat. Phys. **51**, 1091 (1988).

[8] *On Growth and Form*, edited by H. E. Stanley and N. Ostrowsky (Nijhoff, Dordrecht, 1986).

[9] C. S. Lent and P. I. Cohen, Surf. Sci. **139**, 121 (1984); J. M. Pimbley and T.-M. Lu, J. Appl. Phys. **57**, 1121 (1985).

[10] J. M. Pimbley and T.-M. Lu, J. Appl. Phys. **55**, 182 (1984). If $h(r)$ is the height above some *reference* vicinal surface, then here random walk ideas imply that $\langle |h(r)-h(0)|^2 \rangle \sim |r|/w$, where w is the average terrace width.

[11] T.-M. Lu, G. C. Wang, and M. G. Lagally, Surf. Sci. **108**, 494 (1981); J. M. Pimbley and T.-M. Lu, J. Appl. Phys. **57**, 4583 (1985); **59**, 2439 (1986).

[12]J. M. Van Hove, C. S. Lent, P. R. Pukite, and P. I. Cohen, J. Vac. Sci. Technol. B **1**, 741 (1983); E. Bauer, in *RHEED and Reflection Energy Imaging of Surfaces,* edited by P. K. Larsen (Plenum, New York, in press); S. T. Purcell, B. Heinrich, and A. S. Arrott, Phys. Rev. B **35**, 6458 (1987); J. Vac. Sci. Technol. B **6**, 794 (1988); M. J. Henzler and M. Horn, J. Cryst. Growth **81**, 428 (1987).

[13]D. K. Flynn, W. Wang. S.-L. Chang, M. C. Tringides, and P. A. Thiel, Langmuir **4**, 1096 (1988).

[14]D. K. Flynn, J. W. Evans, and P. A. Thiel, J. Vac. Sci. Technol. A (to be published); J. W. Evans, D. K. Flynn, and P. A. Thiel, Ultramicrosc. (to be published).

[15]The analogous result for submonolayer filling processes has been noted previously. See, e.g., J. W. Evans and R. S. Nord, Phys. Rev. A **31**, 3831 (1985).

[16]E. G. D. Cohen, Physica **28**, 1025 (1962).

[17]D. Stauffer, Phys. Rep. **54**, 1 (1979); D. Stauffer, A. Coniglio, and M. Adam, in *Advances in Polymer Science* (Springer-Verlag, Berlin, 1982), Vol. 44.

[18]Note that *all* layers in the sc(100) model of Sec. II have random statistics. Thus random percolation theory applies for *all* $j \geq 1$.

[19]J. W. Evans and D. E. Sanders, J. Vac. Sci. Technol. A **6**, 726 (1988); D. E. Sanders and J. W. Evans, Phys. Rev. A **38**, 4186 (1988).

[20]H. E. Stanley, R. J. Reynolds, S. Redner, and F. Family, in *Real-Space Renormalization,* Vol. 30 of *Current Physics,* edited by T. W. Burkhardt and J. M. J. van Leeuwen (Springer, Berlin, 1982).

[21]H. Saleur and B. Derrida, J. Phys. (Paris) **46**, 1043 (1985).

[22]Consider clusters of empty layer j sites connected by NN bonds. Let Θ_j^* denote associated percolation thresholds, and set $\delta\Theta_j^* = \Theta_j^* - \Theta_1^*$. We obtain 2×2 cell RSRG estimates of $\delta\Theta_2^* = 0.003$, $\delta\Theta_3 = -0.010$, and FSS estimates of $\delta\Theta_2^* = 0.002 \pm 0.001$, $\delta\Theta_3^* = -0.004 \pm 0.002$, $\delta\Theta_4^* = 0.003 \pm 0.002$. The exact Θ_1^* equals $1-\Theta_1^c$ or 0.407.

[23]A. Bonissent in *Crystals: Growth, Properties, and Applications,* edited by H. C. Freyhardt (Springer-Verlag, Berlin, 1983), Vol. 9.

[24]D. E. Sanders (unpublished simulation estimate); J. W. Evans, J. Math. Phys. **25**, 2527 (1984) provides an analytic estimate of 37.5%.

[25]J. W. Evans, D. R. Burgess, and D. K. Hoffman, J. Math. Phys. **25**, 3051 (1984).

[26]Let P_2 (P_2') denote the probability of finding an empty layer-2 site with an empty (filled) layer-1 site beneath it. Then $\Theta_2 = 1 - P_2 - P_2'$, and one can show that $P_2(kt) = e^{-2kt}\{1 + \int_0^{kt} ds \exp[-3s - 2(e^{-s}-1)]\}$ and $P_2' = e^{-kt}\int_0^{kt} ds\, e^s P_2(s)$.

[27]J. W. Evans (unpublished).

[28]J. M. Pimbley and T.-M. Lu, Surf. Sci. **138**, 360 (1984).